THE CHEMICAL, RADIATIVE, AND DILUTIVE EFFECTS OF CO_2 ADDITION ON SOOT FORMATION IN JET A-1 KEROSENE CO-FLOW DIFFUSION FLAME

Yu YANG[1,2#], Qing LI[1#*], Jiajian ZHU[1], Bo ZHOU[3]

[1] College of Aerospace Science and Engineering, National University of Defense Technology, Hunan 410073, China

[2] National Engineering Research Center of New Energy Power Generation, North China Electric Power University, Beijing 102206, China

[3] Department of Mechanics and Aerospace Engineering, Southern University of Science and Technology, Shenzhen 518055, China

[#] These Authors are co-first authors and contributed equally to the work

[*] Corresponding author; E-mail: qing.li@nudt.edu.cn (Q. Li)

With the development of aviation industry, it is urgently to investigate the soot formation properties of aviation kerosene to better control the soot emissions. The dilutive, chemical and radiative effects of CO_2 on the soot inception, condensation and HACA growth processes in laminar co-flow Jet-A1 kerosene diffusion flames were numerically investigated by employing detailed chemical mechanisms and soot sectional models. The results showed that the addition of CO_2 dramatically decreased the maximum temperature (by 92 K) and soot volume fraction (by 41.0%). The dilutive effect of CO_2 contributed the most to the decrease of temperature and soot volume fraction. It also was the main factor in the decrease of soot inception, condensation and HACA growth processes. The chemical effect of CO_2 had little impact on the decomposition of fuels into light hydrocarbons, but obviously limited the growth of light hydrocarbons to A1. The radiative effect of CO_2 decreased the maximum temperature and soot volume fraction by 13 K and 5.2% (from 1.92 to 1.82 ppm). It had little impact on the soot inception, condensation and HACA growth rates.

Key words: *Jet A-1 kerosene diffusion flame, CO_2 addition, chemical effect, radiative effect, soot inception.*

1. Introduction

Recently, soot emission has received considerable attention since it increases the risk of respiratory and cardiovascular diseases for humans and intensifies the greenhouse effect [1]. It is reported that soot emission is mainly attributed to the use of hydrocarbon fuels, such as gasoline and kerosene [2]. With the development of the aviation industry [3, 4], it is urgently to investigate the soot formation properties of kerosene to better control the soot emissions.

Many researchers have experimentally and theoretically studied the soot formation properties in

aviation kerosene combustion. The soot formation was described by the soot inception, condensation, HACA (the hydrogen abstraction acetylene addition) surface growth mechanism and soot oxidation [5]. Among them, the soot inception was the initial process and considered the dominant role in the soot formation processes [6]. Sun et al. [7] experimentally compared the soot formation properties of RP-3 kerosene with that of n-dodecane diffusion flames. They found that the primary particle diameter of n-dodecane was smaller than that of RP-3 since the soot inception was enhanced in RP-3 flame. Saffaripour et al. [8] considered the four-rings pyrolytic aromatic hydrocarbons (A4) as the soot inception precursors for a laminar co-flow Jet-A1 flame. The results showed the modified model was able to predict soot size distributions and structure well comparing with the experimental results. Besides the soot inception, the influence of different chemical mechanisms on the soot condensation in a RP-3 kerosene co-flow diffusion flame was studied by Sun et al. [9]. They found that the C14 n-alkanes mechanism had little effect on the prediction of soot condensation. Abdalla et al. [10] experimentally studied the influence of flow rates on the soot oxidation rate in an inverse RP-3 inverse flame. The results showed that a higher flow rate resulted in a larger amount of VOCs (volatile organic compounds) [11], leading to an increasement in the reactive sites for the oxidizer.

Previous studies have comprehensively revealed the soot formation process in the combustion of aviation kerosene at the atmospheric condition. In the ground experiment, the combustion of hydrocarbon fuels was widely used to obtain the high enthalpy airflow, which produces substantial amounts contaminating species, such as CO_2 and H_2O [12, 13]. The contaminations was proved to have a great impact on the combustion characteristics of aviation kerosene [14]. Liang et al. [15] found that the ignition delay time of RP-3 was inhibited with 10% CO_2 addition at temperatures below 1300 K. The CO_2 addition decreased the formation rate of OH and O radicals through the reactions of $CO_2+O=O_2+CO$ and $CO_2+OH=CO+HO_2$, leading to a suppression effect on the ignition of aviation kerosene. Wang et al. [16] experimentally studied the effect of CO2 on aviation kerosene supersonic combustors. The results showed that the addition of CO_2 reduced the wall pressure by increasing the heat capacities, especially at the equivalence ratio of 0.73. Li et al. [17] found that CO_2 had a nonlinearly reduced influence on the wall pressure in an aviation kerosene supersonic combustion. In addition, they concluded that CO_2 resulted in the decrease of combustion efficiency and streamwise impulse. Previous studies mainly focused on investigating the effect of the CO_2 contamination on the ignition delay time, combustion pressure and efficiency in the aviation kerosene combustion. So far, however, there is much less information about the effect of CO_2 contamination on soot formation in the aviation kerosene flames.

To date, there were several investigations exploring the effect of CO_2 addition on the soot formation in light-hydrocarbon-fueled flames, such as CH_4 and C_2H_4. A numerical analysis was presented to study the formation of soot in CH_4/air co-flow diffusion flames with different CO_2 dilutive ratios [18]. It was observed that the soot loading reduced with the increased CO_2 fraction. A similar trend can be found in a C_2H_4/air co-flow diffusion flame with CO_2 addition [19]. To comprehensively reveal the chemical and dilutive effects of CO_2 on the soot formation, the fictitious CO_2 as a substitute for the real CO_2 was proposed by Liu et al. [20]. They found the reactions $CO_2+H=CO+OH$ and $CO_2+CH=HCO+CO$ were responsible for the chemical effect of CO_2 addition. Guo and Smallwood [19] found that the chemical effect of CO_2 reduced the concentration of H radical, which consequently decreased the soot inception and soot surface growth rates. However, the chemical effect of CO_2 on soot oxidation was negligible [19]. Naseri et al. [23] concluded that chemical effect

of CO_2 limited the PAHs formation through limiting the formation C_2H_2 and C_6H_6, which are building blocks of PAHs. In addition to the chemical and dilutive effects, the radiative effect can not be ignored [21, 22]. Liu et al. [23] reported that the radiative effect of H_2O lowered the temperature in the centerline region by 12 K. Considering the Plank mean absorption coefficients of CO_2 at temperatures above 500 K were larger than those of H_2O [24], it is necessary to explore the radiative effect of CO_2 on the soot formation in the aviation kerosene combustion.

The aim of this paper was to numerically investigate the different effects of CO_2 addition to the airflow on the soot formation in a laminar co-flow Jet-A1 kerosene diffusion flame. The fictitious CO_2 was introduced to isolate the chemical, dilutive and radiative effects. Detailed soot sectional model and chemical mechanism were adopted to analysis the different effect of CO_2 on the soot formation processes. This study firstly and comprehensively revealed the chemical, dilutive and radiative effects of CO_2 addition on soot nucleation, condensation and HACA surface growth in the aviation kerosene flame, which provided a theoretical basis for developing soot emissions-reduction schemes in aviation kerosene combustion.

2. Computational details

The laminar co-flow Jet A-1 kerosene diffusion flames were simulated in the Yale burner[8], which has an inner diameter of 11 mm and 102 mm for the fuel tube and the concentric annular air tube, respectively. The n-decane ($C_{10}H_{22}$), n-propylcyclohexane (C_9H_{18}) and n-propylbenzene (C_9H_{12}) were regarded as the surrogates for the Jet A-1 kerosene [8]. The flow rates of the fuels were set as 23.5 cm/s referring to [8] in all cases. The inlet air velocity was set as 20.1 cm/s in case 1 but 23.1 cm/s in cases 2~4 since 15 vol% CO_2 or fictitious CO_2 was added to the air flow. The inlet temperature of fuel and air flows were 473 K and 423 K. The mole fractions of species in the fuel and air flows are listed in Table 1.

As shown in Table 1, four different cases were simulated. To isolate the chemical, radiative and dilutive effects of CO_2 on the flame properties, two fictitious species $F1CO_2$ and $F2CO_2$ were introduced. Both species had the same transport and thermochemical properties as real CO_2. $F1CO_2$ was allowed to participate in radiation but was chemically inert, and $F2CO_2$ was both chemically and radiatively inert. Comparisons between Cases 1 and 2 containing all the effects of CO_2 addition. Cases 2 and 3 were compared to isolate the chemical effect of CO_2, while the radiative effect of CO_2 was quantified through a comparison between Cases 3 and 4. Moreover, the dilutive effect of CO_2 addition was obtained by comparing the results of Cases 1 and 4.

Table 1. The mole fractions of species in the fuel and air flows.

Cases	Fuel flow				Air flow				
	$C_{10}H_{22}$	C_9H_{18}	C_9H_{12}	N_2	O_2	N_2	CO_2	$F1CO_2$	$F2CO_2$
1	0.0345	0.0055	0.01	0.95	0.25	0.75	0	0	0
2	0.0345	0.0055	0.01	0.95	0.23	0.68	0.09	0	0
3	0.0345	0.0055	0.01	0.95	0.23	0.68	0	0.09	
4	0.0345	0.0055	0.01	0.95	0.23	0.68	0		0.09

The computational domain was 3.78 cm (radial direction, -*r*) × 11.56 cm (streamwise direction, -*z*) with 80 (-*r*) × 160 (-*z*) control volumes. Non-uniform grids were used and the minimal spatial

resolutions of the mesh were 0.2 mm and 0.3 mm in the radial and streamwise directions, respectively. It was checked that further refinement of the mesh did not result in any change in the results. When the maximum relative variation of soot volume fraction (SVF) over 100 iterations was less than 1×10^{-4}, iterations were considered as converged.

3. Numerical models

The flame code developed by Eaves et al. [25] was used in this study. A detailed soot sectional model [23] was adopted. Soot formation processes including soot inception, condensation, surface growth and oxidation were considered at each section. Soot inception was modeled by the collision of two pyrenes (A4) [26]. The HACA mechanism was adopted to described the soot surface growth and oxidation. The fraction of reactive soot surface sites α was an empirical parameter and was assumed as $\alpha = 0.03$ to ensure that the simulation results matched the experimental results. The condensation process was modeled by the collision between the soot and the A4. The condensation efficiency γ which describes the probability of sticking was set as 0.5 [6]. More computational details can be found in [25].

The chemical mechanism developed by Saffaripour et al. [8] was introduced in this study. The radiative properties of CO_2, H_2O were obtained via the statistical narrow-band correlated-k method (SNBCK) with 9 bands ranging 150~9300 cm^{-1}. The Rayleigh expression [27] was adopted to calculated the absorption coefficient of soot. The discrete ordinate method (DOM) with T3 quadrature scheme [28] was used to solve the RTE.

4. Validation of models

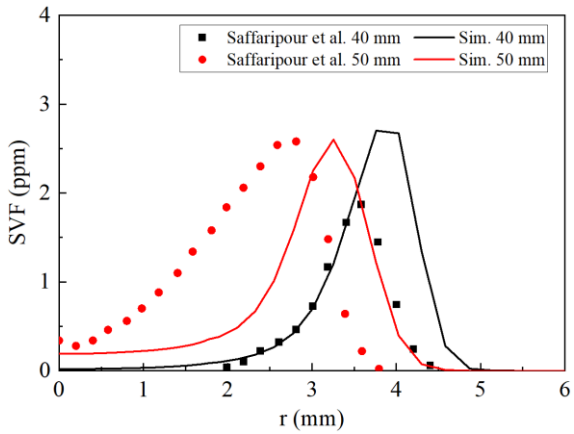

Fig. 1. The comparison of simulated and experimental radial profile of SVF at heights of 40 and 50 mm.

To validate the models used in this study, the simulated radial profile of SVF at heights of 40 and 50 mm in Case 1 were compared with the experimental results introduced from Ref. [8]. As shown in Fig. 1, the simulated SVFs first increased and then decreased with the increase of radius at heights of 40 and 50 mm, agreed well with those of experimental SVFs. The maximum simulated SVF at height of 40 mm was 2.7 ppm larger than that of experimental SVF (1.9 ppm). At height of 50 mm, both the maximum simulated and experimental SVFs were 2.6 ppm. The discrepancies between the experimental and simulated results were attributed to oversimplified soot inception model [29], which

was assumed to be the collision of two A4s. Generally, the models used in this study were validated for modeling co-flow diffusion Jet A-1 kerosene flames.

5. Results and discussion

5.1. The effects of CO_2 on temperature

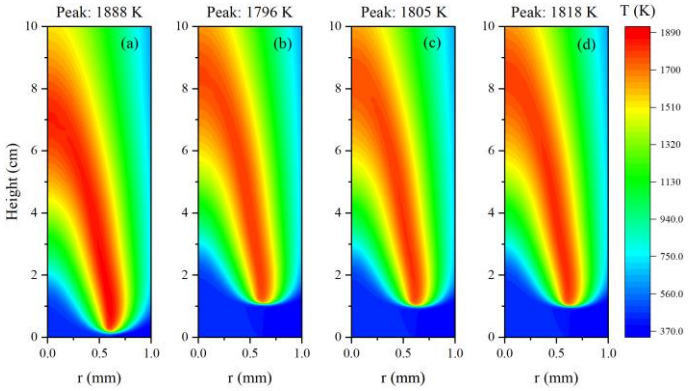

Fig. 2. The temperature distributions of (a) Case1, (b) Case 2, (c) Case 3 and (d) Case 4.

Simulated 2D temperature distributions and peak temperatures of all cases were compared in Fig. 2. In Fig. 2(a-b), the addition of 15 vol% CO_2 had a significant suppression effect on the peak temperature (by 92 K). In addition, the flame was lifted by around 10 mm in Case 2 since the CO_2 addition led to a longer ignition delay time. The dilutive effect of CO_2 addition also caused an obvious drop in the maximum temperature by 70 K, as shown in Fig. 2(a) and (d). The radiative and chemical effects of CO_2 addition resulted in a modest drop in the maximum temperature by 13 K (see Fig. 2(c) and (d)) and 9 K (see Fig. 2(b) and (c)), respectively. The radiative effect of CO_2 on the drop of temperature was due to high radiation ability of CO_2, which resulted in high radiative heat loss. In addition, a lifted distance of 10 mm can also be observed in Cases 3 and 4 shown in Fig. 2 (c) and (d).

5.2. The effects of CO_2 on soot formation

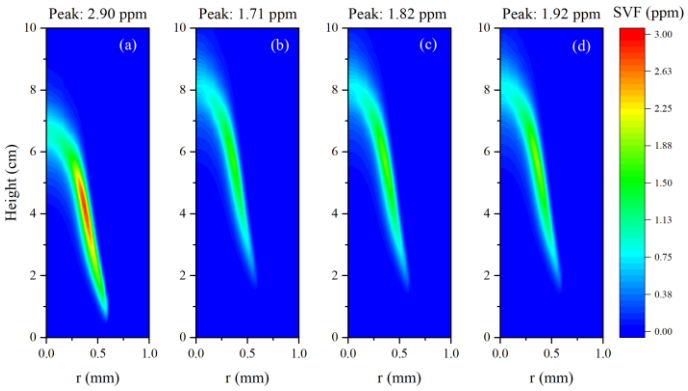

Fig. 3. The SVF distributions of (a) Case1, (b) Case 2, (c) Case 3 and (d) Case 4.

The SVF distributions of four different flames were presented in Fig. 3. It can be seen from Fig. 3(a) and (b) that the soot formation was greatly suppressed by the total effect of CO_2 addition (includes chemical, diluted and radiative effects), with the maximum SVF decreased from 2.9 to 1.71

ppm (by 41.0%). In Fig. 3(a) and (d), the dilutive effect of CO_2 decreased the maximum SVF by 0.98 ppm (by 33.85%), which contributed the most to the drop of SVF compared to the radiative and chemical effects. The reason was that the dilutive effect markedly lowered flame temperature shown in Fig. 2. The radiative effect of CO_2 lowered the maximum SVF from 1.92 ppm in Fig. 3(d) to 1.82 ppm in Fig. 3(c), with a drop of 5.2%. This could be explained by the decrease of temperature caused by the radiative heat loss of CO_2. The chemical effect of CO_2 resulted in a decline of maximum SVF by 0.11 ppm (by 6.0%), depicted in Fig. 3(c) and (d). As mentioned above, the soot formation including soot inception, condensation and HACA surface growth. To comprehensively reveal different effects of CO_2 on different soot formation processes, the soot inception, condensation and HACA surface growth rates at the heights of 0.5, 1.5 and 3.0 cm in Case 1 were discussed following. Since the flames were lifted around 10 mm in Cases 2~4, the results at heights of 1.5, 2.5 and 4.0 cm for Cases 2~4 were compared with those at heights of 0.5, 1.5 and 3.0 cm in Case 1. It was noted that the heights indicated hereinafter refer to those in Case 1.

5.2.1. The effect of CO_2 on soot inception

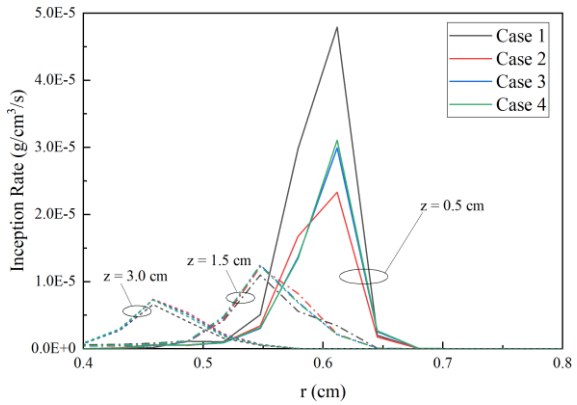

Fig. 4. The radial profile of inception rate at heights of 0.5, 1.5 and 3.0 cm.

As shown in Fig. 4, the soot inception mainly happened at the lower region of the flame. The inception rates at height of 0.5 cm were obviously larger than those at heights of 1.5 and 3.0 cm. The differences in soot inception rates among the four cases at heights of 1.5 and 3.0 cm were quite modest. While at height of 0.5 cm, the CO_2 addition caused the maximum inception rate falling from 4.8e-5 g/cm^3/s (Case 1) to 2.3e-5 g/cm^3/s (Case 2), a decrease of 52.1%. The dilutive played the most important role in the drop of inception rates, leading to a decrease of 1.7e-5 g/cm^3/s (35.4%) by comparison of maximum inception rates for Cases 1 and 4. The difference between the maximum inception rates in Cases 2 and 3 illustrated that the chemical effect of CO_2 had a significant suppression effect on the soot inception rate, with a decrease of 0.7e-5 g/cm^3/s (23.3%). However, the comparison between Cases 3 and 4 showed that the radiative effect of CO_2 on the soot inception rate can be ignored.

The soot inception was modeled by the collision of two A4s in this study. The radial profile of mole fraction of A4 were depicted in Fig. 5(b). It was clear that the A4 showed a similar profile with the inception rates at three heights for all cases. The dilutive and chemical effects of CO_2 caused the 22.7% and 11.8% decrease in the maximum mole fraction of A4, less than those of inception rates (35.4% and 23.3%). That indicated the inception rate not only depended on the A4 mole fraction, but

also on the temperature shown in Fig. 2.

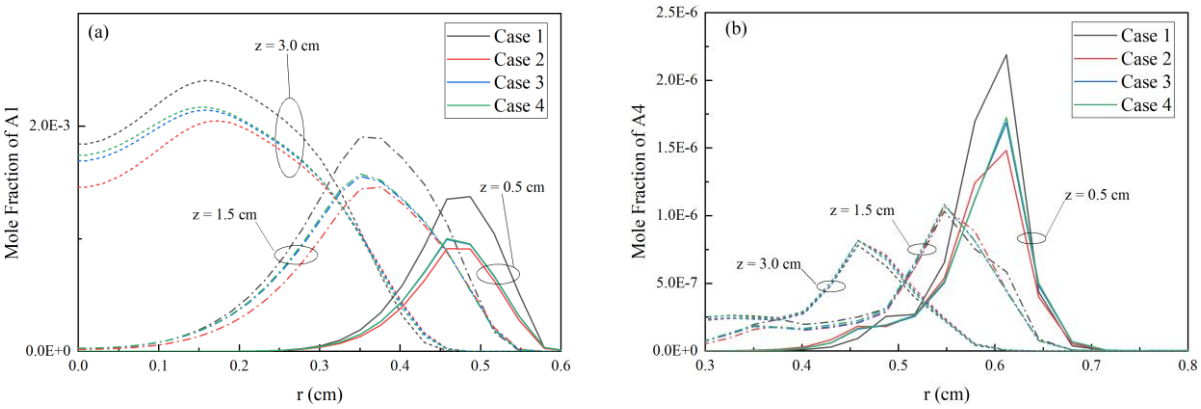

Fig. 5. The radial profiles of mole fraction of A1 and A4 at heights of 0.5, 1.5 and 3.0 cm.

The benzene (A1) was the first ring-structure species and dominated the formation of A4 [23]. The radial profile of mole fraction of A1 were depicted in Fig. 5(a). It was shown that the maximum mole fraction of A1 increased and its location shifted to the centerline region as the height increasing. The CO_2 addition reduced the mole fraction of A1 at three different heights. Once again, the dilutive effect of CO_2 contributed the most effect on the decrease of mole fraction of A1, and the chemical effect of CO_2 was the secondary factor. The dilutive effect of CO_2 on the decrease of mole fraction of A1 could be explained by two reasons. One was the difference in heat capacity between CO_2 and air, which lowered the flame temperature (see Fig. 2(a) and (d)) and consequently limited the reaction rates participting in the formations of PAHs. The other one was the oxygen dilutive caused by the CO_2 addition. Decreacsing oxygen concentration would supressed the growth of PAHs [6]. To further explain the chemical effect of CO_2 on the A1 formation, the integral reaction rates of reactions participating in A1 formation over the whole computational domain were calculated by:

$$\alpha = 2\pi \int_0^z \int_0^r S r dr dz \tag{1}$$

where S was the reaction rate at the given location.

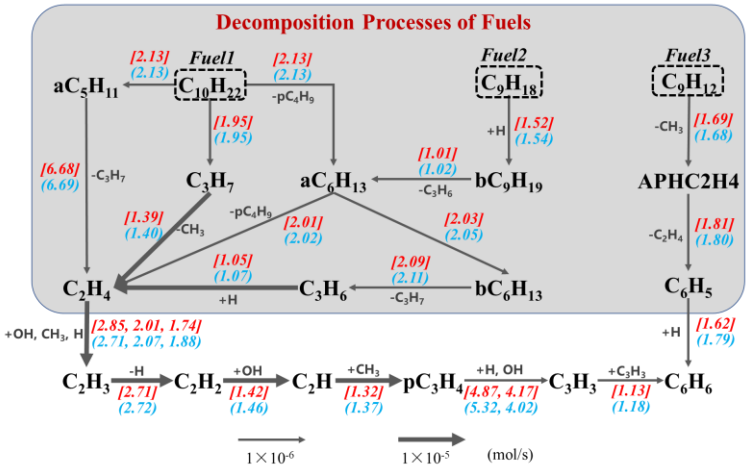

Fig. 6. The formation pathways of A1, the values in square bracket and parenthesis indicate the integral rates for Cases 2 and 3, respectively.

The A1 formation pathways were displayed in Fig. 6 based on the αs in Cases 2 and 3. It was

clear that the A1 formation processes can be divided into two stages: the decomposition of fuels into light hydrocarbons and the growth of light hydrocarbons to A1. For the $C_{10}H_{22}$ and C_9H_{18}, the C_2H_4 was the most important product which grew into the A1 through the pathway of $C_2H_4 \rightarrow C_2H_3 \rightarrow C_2H_2 \rightarrow C_2H \rightarrow pC_3H_4 \rightarrow C_3H_3 \rightarrow C_6H_6$. Another significant A1 formation mechanism was the H-addition reaction of C_6H_5, which was the main decomposition product of the C_9H_{12}.

The integral reaction rates for Cases 2 and 3 were compared in Fig. 6 to investigate how the chemical effect of CO_2 affected the A1 formation. It was clear that the chemical effect of CO_2 reduced the αR1421 ($C_6H_5+H=C_6H_6$) by 0.12e-6 mol/s (from 1.79e-6 to 1.62e-6 mol/s), which dominated on the decrease of A1 mole fraction. The yield of C_6H_5 was mainly through the decomposition reaction of APHC2H4 (R1497: $APHC2H4=C_6H_5+C_2H_4$). As shown in Fig. 6, little discrepancy can be found between the αR1497 in Cases 2 (1.81e-6 mol/s) and 3 (1.80e-6 mol/s). This implied the chemical effect of CO_2 on the C_6H_5 formation could be neglected, which demonstrated that C_6H_5 was not the reason for the decrease of αR1421. The H radical was the other reactant in the R1421 and its radial profile of mole fraction at heights of 0.5, 1.5 and 3.0 cm were ploted in Fig.7(a). It was obvious that the H radical mole fractions at three heights in Case 2 less than those in Case 3. Hence, it can be concluded that the chemical effect of CO_2 decreased the H radical mole fraction, subsequently lowering the reaction rate of R1421, resulting in the drecrease of the A1 mole fraction.

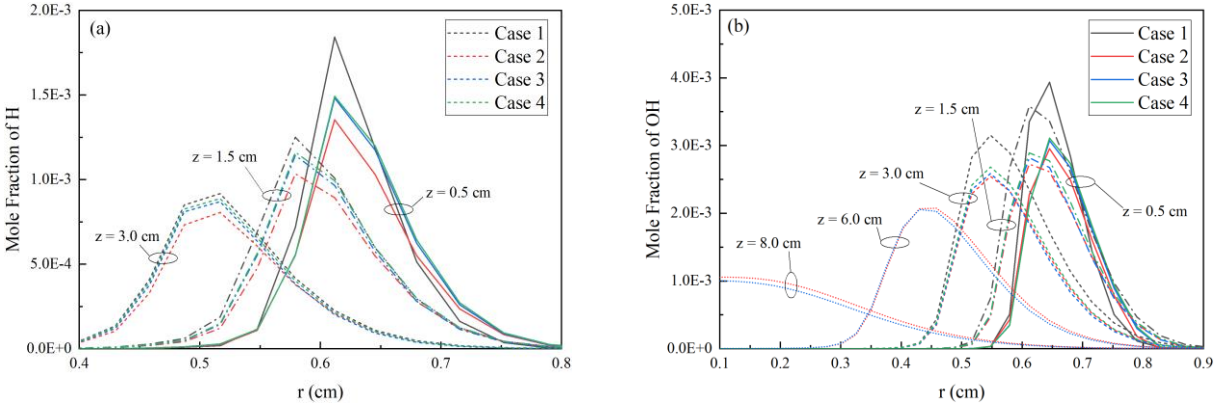

Fig. 7. The radial profiles of mole fraction of H and OH at heights of 0.5, 1.5 and 3.0 cm.

The decrease of αR230 ($2C_3H_3=C_6H_6$) by 0.05e-6 mol/s was the other factor contributing to the decrease of A1 mole fraction. There were two primary channels that contribute to the formation of C_3H_3. One was the H-abstraction reaction of pC_3H_4 with H radical (R681: $pC_3H_4+H=C_3H_3+H_2$). The other was the H-abstraction reaction of pC_3H_4 with OH radical (R671: $PC_3H_4+OH=C_3H_3+H_2O$). As manifested in Fig. 6, the chemical effect of CO_2 resulted in a decrease of αR681 by 0.45e-6 mol/s, but an increase of αR671 by 0.15e-6 mol/s. As indicated in Fig. 7(a), the decrease of H radical was responsible for the decrease of αR681. The radial profile of mole fraction of OH at heights of 0.5, 1.5 and 3.0 cm were depicted in Fig. 7(b) to illustrate the increase of αR671. Surprisingly, the chemical effect of CO_2 reduced the OH mole fractions at heights of 0.5, 1.5 and 3.0 cm, which were inconsistent with the change of αR671. However, it can be observed in Fig. 7(b) that the difference of OH mole fraction between Cases 2 and 3 had became smaller as the height increased. The OH mole fraction in Case 2 was even a little larger than that in Case 3 at height of 3.0 cm where the radius was larger than 0.6 cm. Further, the radial profile of mole fraction of OH at heights of 6.0 and 8.0 cm for Cases 2 and 3 were also plotted in Fig. 7(b). Obviously, the chemical effect of CO_2 caused an increase of OH mole fraction at heights of 6.0 and 8.0 cm. This demonstrated the increase of OH mole fraction at higher

region of flame was the dominant role in the rise of αR671.

The C_2H_4, as the key intermediate product of $C_{10}H_{22}$ and C_9H_{18}, was the initial precursor for the A1 formation. As shown in Fig. 6, the chemical effect of CO_2 did not affect the formation reactions of C_2H_4. That was mainly caused by the little difference in the decomposition processes of $C_{10}H_{22}$ and C_9H_{18} between Cases 2 and 3. The yield of C_2H_3 mainly through R419 (C_2H_4+OH=C_2H_3+H_2O), R425 (C_2H_4+CH_3=C_2H_3+CH_4) and R422 (C_2H_4+H=C_2H_3+H_2). The chemical effect of CO_2 increased the αR419 by 0.14e-5 mol/s, but decreased the αR425 and αR422 by 0.06e-5 and 0.14e-5 mol/s. The decrease of formation rate of C_2H_3 eventually limited the C_6H_6 formation through C_2H_3→C_2H_2→C_2H →pC_3H_4→C_3H_3→C_6H_6.

In general, the chemical effect of CO_2 caused little difference in the decomposition processes of $C_{10}H_{22}$, C_9H_{18} and C_9H_{12}. The decrease of H mole fraction caused by the chemical effect of CO_2 resulted in the decrease of A1 mole fraciton through R1421. The decrease of αR230 was the other factor contributing to the decrease of A1 mole fraction, which was initially caused by the decrease of C_2H_3 formation through R422 and R425.

5.2.2. The effect of CO_2 on soot condensation and HACA surface growth

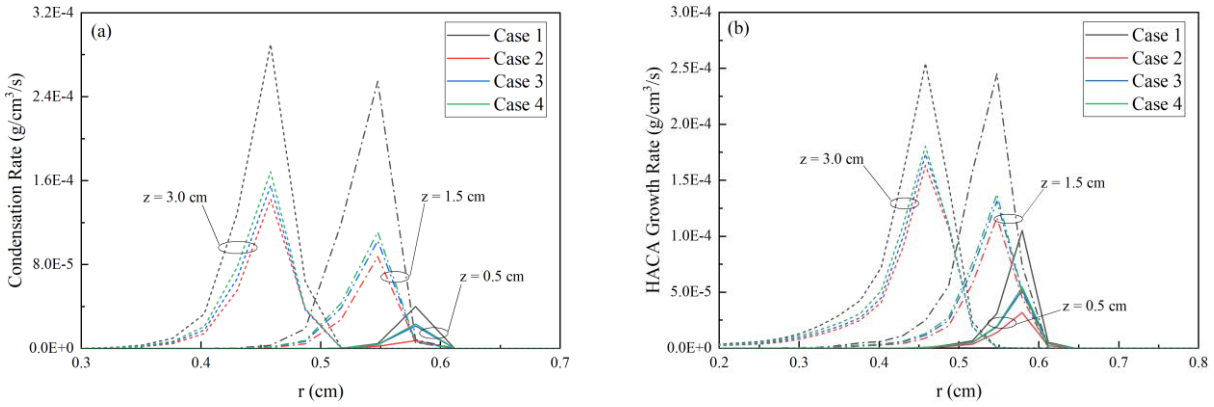

Fig. 8. The radial profiles of condensation and HACA growth rates at heights of 0.5, 1.5 and 3.0 cm.

The different effects of CO_2 addition on the soot condensation rate at heights of 0.5, 1.5 and 3.0 cm were plotted in Fig. 8(a). Unlike the soot inception, the soot condensation rates at heights of 1.5 and 3.0 cm were higher than those at 0.5 cm. This implied the soot condensation happened at a higher region of the flame. Comparing Cases 1 and 2, the CO_2 addition dramatically limited the soot condensation at three different heights. At height of 3.0 cm, the dilutive effect of CO_2 lowered the maximum soot condensation rate by 42.1% (from 2.90e-4 to 1.68e-4 g/cm^3/s), comparing Cases 1 and 4. The chemical and radiative effect of CO_2 showed a similar ability to suppress the soot condensation. The chemical effect of CO_2 decreased the maximum soot condensation rate at height of 3.0 cm by 8.4% (from 1.55e-4 to 1.42e-4 g/cm^3/s), which was larger than the radiative effect of CO_2 (by 7.7%, from 1.68e-4 to 1.55e-4 g/cm^3/s). The condensation process was modeled by the collision between the soot and A4. Thus, it depended on the temperature and the mole fraction of soot and A4. As discussed in section 5.2, the chemical and radiative effect of CO_2 lowered the temperature, leading to the decrease of soot condensation. The soot inception was the first process in the soot formation and providing the precursor (soot) for the condensation process. The soot inception was limited by the

chemical effect of CO_2, but little limited by the radiative effect of CO_2, see Fig. 4. This illustrated that the chemical effect of CO_2 (8.4%) had a more dramatic impact on the soot condensation than the radiative effect of CO_2 (7.7%).

The different effects of CO_2 addition on the HACA growth rates at heights of 0.5, 1.5 and 3.0 cm were plotted in Fig. 8(b). Similar to the soot condensation, the CO_2 addition dramatically suppressed the HACA growth rate. The dilutive effect of CO_2 contributed the most effect on the decrease of the HACA growth rate, followed by the chemical effect of CO_2, but the radiative effect of CO_2 was small.

6. Conclusions

The effects of CO_2 addition to the air flow on the laminar co-flow Jet A-1 kerosene diffusion flame were numerically studied by employing detailed soot sectional models and a detailed chemical mechanism. Four different cases were investigated to isolate the dilutive, chemical and radiative effects of CO_2 on the soot inception, condensation and HACA growth rates. Following were the main conclusions:

(1) The addition of 15 vol% CO_2 had a significant suppression effect on the temperature and soot formation. It dramatically decreased the peak temperature by 92 K and decreased the maximum soot mole fraction by 41.0% (from 2.90 to 1.71 ppm).

(2) The dilutive effect of CO_2 contributed the most effect on the decrease of temperature and soot mole fraction. Moreover, it was the main factor in the decrease of soot inception, soot condensation and HACA growth rates. The chemical effect of CO_2 was the secondary factor.

(3) The chemical effect of CO_2 had little influence on the decomposition of fuels into light hydrocarbons, but obviously limited the growth of light hydrocarbons to A1.

(4) The radiative effect of CO_2 decreased the maximum temperature and soot mole fraction by 13 K and 5.2% (from 1.92 to 1.82 ppm), respectively. It had little impact on the soot inception, soot condensation and HACA growth rates.

Acknowledgements

This work was supported by the National Natural Science Foundation of China (No. 51976057).

Nomenclature

Variables

α - the integral reaction rate over the whole computational domain, [mol/s]

S - the reaction rate at the given location, [mol/cm^3/s]

f_v - the soot volume fraction [-]

Acronyms

DOM - the discrete ordinate method

HACA - the hydrogen abstraction acetylene addition

RTE - the radiative transfer equation

SNBCK - the statistical narrow-band correlated-k method

References

[1] Zhao T, Fang J,Huang Z. The evolution of soot morphology for the maturation of nascent particle in a turbulent lifted jet flame. *Thermal Science*, 2022(00): p. 57-57.

[2] Wang Y,Chung SH. Soot formation in laminar counterflow flames. *Progress in Energy and Combustion Science*, 2019. 74: p. 152-238.

[3] Feng R, Huang Y, Zhu J, Wang Z, Sun M, Wang H,Cai Z. Ignition and combustion enhancement in a cavity-based supersonic combustor by a multi-channel gliding arc plasma. *Experimental Thermal and Fluid Science*, 2021. 120: p. 110248.

[4] Feng R, Zhu J, Wang Z, Zhang F, Ban Y, Zhao G, Tian Y, Wang C, Wang H,Cai Z. Suppression of combustion mode transitions in a hydrogen-fueled scramjet combustor by a multi-channel gliding arc plasma. *Combustion and Flame*, 2022. 237: p. 111843.

[5] Ju H, Bian F,Wei M. Modeling of soot particle collision and growth paths in gas-solid two-phase flow. *Thermal Science*, 2021. 25(5 Part B): p. 3741-3752.

[6] Jerez A, Consalvi J-L, Fuentes A, Liu F,Demarco R. Soot production modeling in a laminar coflow ethylene diffusion flame at different Oxygen Indices using a PAH-based sectional model. *Fuel*, 2018. 231: p. 404-416.

[7] Sun M, Gan Z,Yang Y. Numerical and experimental investigation of soot precursor and primary particle size of aviation fuel (RP-3) and n-dodecane in laminar flame. *Journal of the Energy Institute*, 2021. 94: p. 49-62.

[8] Saffaripour M, Veshkini A, Kholghy M,Thomson MJ. Experimental investigation and detailed modeling of soot aggregate formation and size distribution in laminar coflow diffusion flames of Jet A-1, a synthetic kerosene, and n-decane. *Combustion and Flame*, 2014. 161(3): p. 848-863.

[9] Sun M, Gan Z,Yang Y. A Comparison Study of Soot Precursor and Aggregate Property Between Algae-Based Aviation Biofuel and Aviation Kerosene RP-3 in Laminar Flame. *Journal of Energy Resources Technology*, 2021. 143(11).

[10] Abdalla AO, Liu D, Zhang L, Zhao X, Ying Y, Jiang B,He X. Soot formation and evolution in RP-3 kerosene inverse diffusion flames: Effects of flow rates and dimethyl carbonate additions. *Fuel*, 2020. 273: p. 117732.

[11] Sui R, Mantzaras J, Liu Z,Law CK. Kinetic modeling of total oxidation of propane over rhodium. *Combustion and Flame*, 2021: p. 111847.

[12] Choubey G, Yuvarajan D, Huang W, Yan L, Babazadeh H,Pandey K. Hydrogen fuel in scramjet engines-A brief review. *International Journal of Hydrogen Energy*, 2020. 45(33): p. 16799-16815.

[13] Zheng S, Liu H, Li Q, Zhu J, Sun M, Zhou B, Sui R,Lu Q. Effects of radiation reabsorption on the laminar flame speed and NO emission during aviation kerosene combustion at elevated pressures. *Fuel*, 2022. 324: p. 124545.

[14] Pellett G, Bruno C,Chinitz W. Review of air vitiation effects on scramjet ignition and flameholding combustion processes. in *38th AIAA/ASME/SAE/ASEE Joint Propulsion Conference & Exhibit*. 2002.

[15] Liang J-H, Wang S, Zhang S-T, Yue L-J, Fan B-C, Zhang X-Y,Cui J-P. The vitiation effects of water vapor and carbon dioxide on the autoignition characteristics of kerosene. *Acta Mechanica Sinica*, 2014. 30(4): p. 485-494.

[16] Wang Y, Song W, Fu Q, Shi D,Wang Y. Experimental study of vitiation effects on hydrogen/kerosene fueled supersonic combustor. *Aerospace Science and Technology*, 2017. 60: p. 108-114.

[17] Li J, Song W, Luo F,Chen L. Numerical investigation of H2O and CO2 vitiation effects on kerosene-fueled supersonic combustion. *Journal of Propulsion Technology*, 2013. 34: p. 563-571.

[18] Samanta A, Ganguly R,Datta A. Effect of CO2 dilution on flame structure and soot and NO formations in CH4-air nonpremixed flames. *Journal of Engineering for Gas Turbines and Power*, 2010. 132(12).

[19] Guo H,Smallwood GJ. A numerical study on the influence of CO2 addition on soot formation in an ethylene/air diffusion flame. *Combustion Science and Technology*, 2008. 180(10-11): p. 1695-1708.

[20] Liu F, Guo H,Smallwood GJ. The chemical effect of CO2 replacement of N2 in air on the burning velocity of CH4 and H2 premixed flames. *Combustion and Flame*, 2003. 133(4): p. 495-497.

[21] Zheng S, Yang Y, Sui R,Lu Q. Effects of C2H2 and C2H4 radiation on soot formation in ethylene/air diffusion flames. *Applied Thermal Engineering*, 2021. 183: p. 116194.

[22] Zheng S, Liu H, Li D, Liu Z, Zhou B,Lu Q. Effects of radiation reabsorption on the laminar burning velocity of methane/air and methane/hydrogen/air flames at elevated pressures. *Fuel*, 2022. 311: p. 122586.

[23] Liu F, Consalvi J-L,Fuentes A. Effects of water vapor addition to the air stream on soot formation and flame properties in a laminar coflow ethylene/air diffusion flame. *Combustion and Flame*, 2014. 161(7): p. 1724-1734.

[24] Rivière P,Soufiani A. Updated band model parameters for H2O, CO2, CH4 and CO radiation at high temperature. *International Journal of Heat and Mass Transfer*, 2012. 55(13-14): p. 3349-3358.

[25] Eaves NA, Zhang Q, Liu F, Guo H, Dworkin SB,Thomson MJ. CoFlame: A refined and validated numerical algorithm for modeling sooting laminar coflow diffusion flames. *Computer Physics Communications*, 2016. 207: p. 464-477.

[26] Wei M, Li S, Liu J,Guo G. Effects of ethanol addition on soot particles dynamic evolution in ethylene/air laminar premixed flame. *Thermal Science*, 2018. 22(3): p. 1339-1350.

[27] Liu F, Guo H,Smallwood GJ. Effects of radiation model on the modeling of a laminar coflow methane/air diffusion flame. *Combustion and Flame*, 2004. 138(1-2): p. 136-154.

[28] Thurgood C, Pollard A,Becker H. The TN quadrature set for the discrete ordinates method. 1995.

[29] Zhang C, Chen L, Ding S, Xu H, Li G, Consalvi J-L,Liu F. Effects of soot inception and condensation PAH species and fuel preheating on soot formation modeling in laminar coflow CH4/air diffusion flames doped with n-heptane/toluene mixtures. *Fuel*, 2019. 253: p. 1371-1377.

Submitted: 04.06.2022.

Revised: 02.08.2022.

Accepted: 11.08.2022.